



A comprehensive experimental and kinetic modeling study of 1-and 2-pentene

Title	A comprehensive experimental and kinetic modeling study of 1-and 2-pentene
Author(s)	Dong, Shijun;Zhang, Kuiwen;Ninnemann, Erik M.;Najjar, Ahmed;Kukkadapu, Goutham;Baker, Jessica;Arafin, Farhan;Wang, Zhandong;Pitz, William J.;Vasu, Subith S.;Sarathy, S. Mani;Senecal, Peter K.;Curran, Henry J.
Publication Date	2020-10-15
Publisher	Elsevier
Repository DOI	10.1016/j.combustflame.2020.09.012



A comprehensive experimental and kinetic modeling study of 1- and 2-pentene

Shijun Dong^{a,*}, Kuiwen Zhang^{b,c}, Erik M. Ninnemann^d, Ahmed Najjar^e,
Goutham Kukkadapu^b, Jessica Baker^d, Farhan Arafin^d, Zhandong Wang^e, William J. Pitz^b,
Subith S. Vasu^d, S. Mani Sarathy^e, Peter K. Senecal^c, Henry J. Curran^a

^a Combustion Chemistry Centre, School of Chemistry, Ryan Institute, MaREI, NUI Galway, Ireland

^b Lawrence Livermore National Laboratory, Livermore, USA

^c Convergent Science, Madison, WI, USA

^d Center for Advanced Turbomachinery and Energy Research (CATER), Department of Mechanical and Aerospace Engineering, University of Central Florida, Orlando, USA

^e King Abdullah University of Science and Technology, Clean Combustion Research Center, Physical Sciences and Engineering Division, Thuwal, Saudi Arabia

ARTICLE INFO

Article history:

Received 12 May 2020

Revised 10 September 2020

Accepted 11 September 2020

Keywords:

1- and 2-pentene
Ignition delay time
NTC
Kinetic model

ABSTRACT

1- and 2-pentene are components in gasoline and are also used as representative alkene components in gasoline surrogate fuels. Most of the available ignition delay time data in the literature for these fuels are limited to low pressures, high temperatures and highly diluted conditions, which limits the kinetic model development and validation potential of these fuels. Therefore, ignition delay time measurements under engine-like conditions are needed to provide target data to understand their low-temperature fuel chemistry and extend their chemical kinetic validation to lower temperatures and higher pressures. In this study, both a high-pressure shock tube and a rapid compression machine have been employed to measure ignition delay times of 1- and 2-pentene over a wide temperature range (600–1300 K) at equivalence ratios of 0.5, 1.0 and 2.0 in 'air', and at pressures of 15 and 30 atm. At high-temperatures (> 900 K), the experimental ignition delay times show that the fuel reactivities of 1- and 2-pentene are very similar at all equivalence ratios and pressures. However, at low temperatures, 1-pentene shows negative temperature coefficient behavior and a higher fuel reactivity compared to 2-pentene. Moreover, carbon monoxide time-histories for both 1- and 2-pentene were measured in a high-pressure shock tube for a stoichiometric mixture at 10 atm and at high temperatures. Furthermore, species versus temperature profiles were measured in a jet-stirred reactor at $\phi = 1.0$ and 1 atm over a temperature range of 700–1100 K. All of these experimental data have been used to validate the current chemistry mechanism. Starting from a published pentane mechanism, modifications have been made to the 1- and 2-pentene sub-mechanisms resulting in overall good predictions. Moreover, flux and sensitivity analyses were performed to highlight the important reactions involved in the oxidation process.

© 2020 The Combustion Institute. Published by Elsevier Inc. All rights reserved.

1. Introduction

Real gasoline fuels can be composed of over a hundred different hydrocarbon species [1]. Therefore, gasoline surrogate models which show similar chemical and physical properties to commercial gasoline have been developed to simulate engine combustion processes. In the development of gasoline surrogate models, generally one or two species are used to represent each of the important hydrocarbon classes in practical gasoline. Alkenes comprise

approximately 2–5% by volume of a typical gasoline [1]. Alkenes show higher research octane numbers compared to their corresponding alkanes and thus can directly affect the auto-ignition behavior, and the unsaturated carbon bond can also contribute to soot formation [2]. To represent the alkene components of practical gasoline, 1- and 2-pentene have been adopted as representative alkene components in some gasoline surrogate models [1–5].

Therefore, it is important to understand the fuel chemistry of 1- and 2-pentene. A few studies have measured ignition delay times (IDTs) [6–9] and flame speeds [10] for both 1- and 2-pentene, and a few kinetic models have also been developed [6,7]. Touchard et al. [7] measured IDTs for 1-pentene at high temperatures (1130–

* Corresponding author.

E-mail address: shijun.dong@nuigalway.ie (S. Dong).

Table 1

Experimental conditions of the IDT data for 1- and 2-pentene available in the literature.

T (K)	p (atm)	ϕ	X_{fuel} (%)	Fuel studied	Reference
700–900	8	1.0	2.72	1-pentene	Ribaucour et al. [6]
1130–1620	8.5	0.5, 1.0, 2.0	1, 2	1-pentene	Touchard et al. [7]
1100–1950	1, 10	0.5, 1.0, 2.0	1, 2.8	1- and 2-pentene	Mehl et al. [8]
1040–1880	1, 10	0.5, 1.0, 2.0	0.5, 1.0	1-pentene	Cheng et al. [9]
600–1300	15, 30	0.5, 1.0, 2.0	1.38, 2.72, 5.44	1- and 2-pentene	Current study

1620 K) at a pressure of 8.5 atm in a shock tube, and a kinetic model describing the high temperature oxidation of 1-pentene was developed using the EXGAS software. Mehl et al. [8] and Cheng et al. [9] also recorded IDT data for 1- and 2-pentene in shock tubes, with most of these data recorded for highly dilute mixtures at pressures of less than 10 atm. Table 1 shows the experimental conditions for all of the IDT data for 1- and 2-pentene available in the literature and measured in the current study. X_{fuel} represents the fuel percentage in the mixture. As can be seen, most of the IDT data for 1- and 2-pentene in the literature were taken at low pressures (less than 12 atm), and only two data sets were taken under fuel in ‘air’ conditions with the remainder taken under highly-diluted conditions (~1% fuel concentration). As a consequence, measured IDTs in shock tubes are restricted to high temperatures, > 1000 K. In this study, IDTs were measured for fuel mixtures in ‘air’ at higher pressures, thus the high-pressure shock tube (HPST) experiments were extended to lower temperatures. Ribaucour et al. [6] studied the auto-ignition behavior of 1-pentene in a rapid compression machine (RCM), and observed a less pronounced negative temperature coefficient (NTC) behavior compared to alkanes. Along with the experimental results, a kinetic model was developed and validated in the low temperature regime (600–900 K). However, Ribaucour et al. [6] only recorded one data set and volume versus time profiles used to simulate RCM facility effects were not provided. Moreover, to the authors’ knowledge, there is no RCM IDT data for 2-pentene available in the literature. Since 1- and 2-pentene are important representative alkene components, IDT data at engine-relevant conditions (fuel in ‘air’, $p > 10$ atm and at relatively low temperatures of 600–1000 K) are essential to validate their low-temperature chemistry. Furthermore, to the authors’ knowledge, there is no jet-stirred reactor (JSR) data available for 1- and 2-pentene in the literature.

Since there is not enough experimental data available at low-temperature conditions, most of previously published 1- and 2-pentene models mainly focused on high-temperature chemistry [6,7,9]. As discussed earlier, 1-pentene shows a less pronounced NTC behavior compared to *n*-pentane, which was not seen for 1-butene, even at higher pressures [11]. As a consequence, from ethylene to 1-heptene, 1-pentene is the first 1-alkene to show NTC behavior which is also observed for 1-hexene [12] and 1-heptene [13]. Therefore, building a 1-pentene kinetics model can help in understanding the low-temperature chemistry of all alkenes. Some published quantum chemistry calculations for alkene chemistry [14–20] has aided our understanding of alkene chemistry. Moreover, since 1- and 2-pentene share potential energy surfaces for important intermediate species and some identical intermediate products (1-penten-3-yl, 1,3-pentadiene, etc.) and also have similar reaction pathways during their oxidation (Waddington mechanism, allyl radicals combination with hydroperoxyl radicals, etc.), consistent rate constants need to be used for 1- and 2-pentene kinetic models. Therefore, it is important to develop the two kinetic models simultaneously. Furthermore, pentenes are important intermediate species formed during the oxidation of pentanes. Some reaction pathways can affect both pentene and pentane chemistry, thus the pentene and pentane models should be validated simultaneously.

Table 2

Experimental conditions studied for both 1- and 2-pentene in the HPST and RCM.

T (K)	p (atm)	ϕ	Dilution (%)
650–1300	15, 30	0.5, 1.0, 2.0	74.8–77.9

In this paper, IDTs of 1- and 2-pentene over a wide temperature range (600–1300 K) and at high pressure (15 and 30 atm) conditions have been measured using both a high-pressure shock tube (HPST) and a rapid compression machine. A JSR has also been used to measure reactant, intermediate and product species profiles for both 1- and 2-pentene oxidation, in the temperature range 700–1100 K, at $\phi = 1.0$ and $p = 1$ atm. Carbon monoxide time-histories for both 1- and 2-pentene were measured in a high-pressure shock tube at high pressures and at high temperatures. Moreover, a kinetic model has been developed based on a published pentane mechanism [21] to capture the auto-ignition behavior as well as species profiles for both 1- and 2-pentene.

2. Experimental specifications

2.1. Ignition delay time measurements

In this study, both a HPST and an RCM at NUI Galway were employed to conduct the experiments. The HPST was used to measure IDTs of less than 3 ms which are too short to be reliably measured in the RCM. A brief description of the facility will be given here as detailed descriptions have been reported previously [22,23]. Detailed descriptions of the facilities are also provided as Supplementary material. The gas temperature and pressure behind the reflected shock wave were calculated using GasEq [24] based on the measured incident shock velocity and initial conditions of temperature, pressure and mixture composition. The compressed gas temperatures in the RCM experiments are calculated using GasEq based on the measured compressed pressure and initial conditions of pressure, temperature, and mixture composition.

As discussed above, IDTs of 1- and 2-pentene have been measured for fuel/‘air’ mixtures at relatively high pressures (15 and 30 atm) over a wide temperature range (600–1300 K). In the experiments, ‘air’ refers to the diluent (nitrogen or argon) and oxygen in a ratio of 79:21. The designed experimental conditions are shown in Table 2.

The definitions of IDTs measured in the HPST and RCM are shown in Fig. 1, which are based on the measured pressure traces in the two facilities. As shown in Fig. 1(b), two-stage ignition behavior was observed in the 1-pentene RCM experiments. The definitions of 1st and 2nd IDT are also shown in Fig. 1(b). As discussed in previous studies [11], a 20% uncertainty is assigned to all of the IDT measurements in both facilities.

High purity 1- and 2-pentene fuels were provided by Sigma-Aldrich. The purity of 1-pentene is > 98.5%, and 2-pentene is a mixture of trans- and cis-2-pentene with a purity higher than 99%. IDT measurements for trans-2-pentene (> 99%) were performed and the results are very close to that of trans- and cis-2-pentene mixture, with the comparison provided in Fig. S3 of the Supplementary material. Therefore, a mixture of trans- and cis-2-pentene

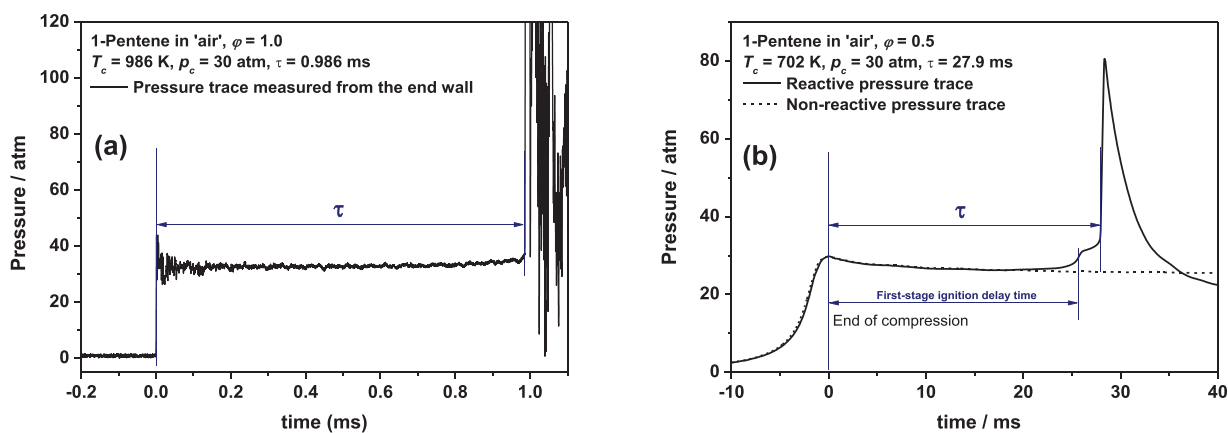


Fig. 1. Definition of ignition delay time measurements in (a) a HPST and (b) an RCM.

has been used for the RCM and HPST experiments. High purity oxygen (> 99%), nitrogen (> 99%) and argon (> 99%) provided by BOC were used in the experiments.

2.2. Species time-histories measurements in a high-pressure shock tube

Carbon monoxide time-histories were measured in a high-pressure shock tube at UCF with detailed descriptions of the facility presented in [25–31]. The velocity of the incident shock wave was measured using five piezoelectric pressure transducers. The temperature (T_5) and pressure (p_5) behind the reflected shock were calculated through quasi one-dimensional normal shock relations using the measured incident shock velocity. Eight equally spaced ports around the circumference of the tube, 2.0 cm from the end-wall, were used for pressure and spectroscopic measurements. 1-pentene was obtained from Sigma-Aldrich ($\geq 99.5\%$ purity), while trans-2-pentene was obtained from Alfa Aesar (99% purity). To measure carbon monoxide time-histories, a continuous wave, distributed feedback quantum cascade laser centered at 2046.30 cm^{-1} from Alpes Lasers (TO3-L-50) was used [32–34]. Detailed descriptions of the laser setup and experiment process are provided as Supplementary material. The correlation for CO absorption cross-section is taken from Ninnemann et al. [35]. Despite using a correlation with temperature and pressure dependence, the temperature rise due to the observed ignition event was not quantified; thus, the CO time-histories are truncated before there is a significant pressure rise. For these experiments, the IDT is defined at the maximum rate of change in pressure due to the ignition event from time zero (minimum of the observed Schlieren spike).

2.3. JSR species profile measurements

The JSR experimental setup in KAUST has been described previously [36]. Reactants (fuels and oxidizer) were introduced to a fused silica spherical reactor (volume 76 cm^3). Perfect mixing was achieved by flowing reactant via four opposing nozzles (ID 0.3 mm) [37]. Detailed descriptions of the facility and experiment process are provided in the Supplementary material. The experiments were performed at a steady state, at a constant pressure of 1 atm with a temperature of 750–1025 K, and a constant mean residence time $\tau = 2 \text{ s}$. A mixture composition of 0.4% fuel/3% O_2 /96.6% N_2 was used for these measurements, corresponding to stoichiometric equivalence ratio. Measurement repeatability was observed to be within 10%, and uncertainty of temperature measurement was determined as 25 K.

Table 3

Major updated reaction classes and references in the current model.

No.	Reaction pathways	Reference
1	$\dot{\text{O}}\text{H}$ addition to C = C double bond	[39]
2	Waddington mechanism, Hydroxy-alkylperoxy radical isomerization and $\text{H}\dot{\text{O}}_2$ elimination	[14]
3	Alkenylperoxy radical isomerization and decomposition	[15,16]
4	Pentene + $\text{H}\dot{\text{O}}_2$	[18]
5	Pentene + H	[19]
6	Isomerization and decomposition of pentenyl radicals	[20]

3. Chemistry mechanism development

Bugler et al. published a chemistry model [38] describing the oxidation of the pentane isomers which contains sub-models for 1-pentene and 2-pentene. However, the low temperature reaction pathways for these alkenes are missing. As discussed above, previous experimental results show that 1-pentene has an NTC behavior, which indicates the importance of low-temperature chemistry. In this paper, significant modifications have been made to the pentene sub-mechanism contained in Bugler et al. [38] mechanism. Moreover, rate constants of some important reaction classes have been updated according to some recent literature studies [14,15,16,18,39]. Some of the important improvements are shown in Table 3 and are discussed in detail below. The thermochemical parameters for the species related to the pentene chemistry were calculated using THERM [40], with updated group values from Burke et al. [41] and Li et al. [42]. A new reaction sub-mechanism, NUIGMech1.0, was used to develop the current model and the final mechanism is available as Supplementary material.

3.1. Low-temperature chemistry

3.1.1. $\dot{\text{O}}\text{H}$ addition to the double bond

It is well known that $\dot{\text{O}}\text{H}$ radical addition to the double bond is one of the most important reaction classes for alkene chemistry, as the hydroxyalkyl radicals so produced can add to molecular oxygen and form hydroxyalkyl-peroxy radicals which can undergo β -

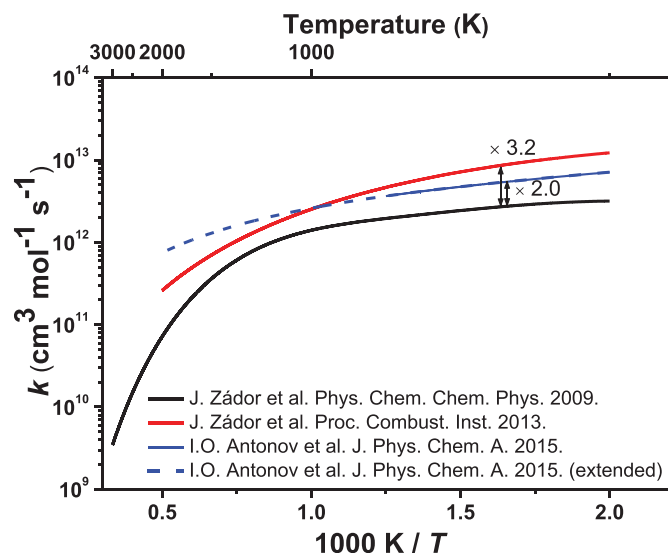
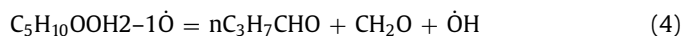
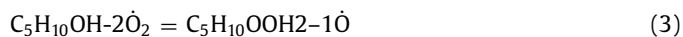
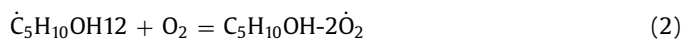


Fig. 2. Comparison of rate constants for $\dot{\text{O}}\text{H}$ addition to the central carbon site of alkenes at 10 atm from the literature [17,39,45].

scission producing aldehydes and hydroxy radicals, which is known as the Waddington mechanism, Eqs. (1)–(4).



In addition to the Waddington reaction pathway, it is also suggested that hydroxyalkyl-peroxy radicals can undergo intramolecular hydrogen transfer reactions, similar to those involved in the low temperature chemistry of alkanes, which can also contribute to low-temperature reactivity [43,44]. Therefore, the rate constants of $\dot{\text{O}}\text{H}$ radical addition to the $\text{C}=\text{C}$ double bond is critically important in predicting low-temperature alkene chemistry. There have been a number of recent experimental and theoretical studies concerning $\dot{\text{O}}\text{H}$ radical addition to the double bond in alkenes [17,39,45]. Zádor et al. [17] studied the reaction of hydroxyl radicals with propene using quantum chemistry calculations. Following this study, they also investigated the rate constants of $\dot{\text{O}}\text{H}$ addition to the double bond of propene in the reverse direction and validated experimental results [45]. Antonov et al. [39] performed a combined experimental and theoretical study of the reaction of $\dot{\text{O}}\text{H}$ with trans-2-butene. Figure 2 shows the comparison of the rate constants of $\dot{\text{O}}\text{H}$ addition to the central carbon site. It can be seen that at 600 K, the rate constants from the experimental study of Zádor et al. [45] (published in 2013) are about a factor of 3.2 higher than their values from their theoretical study published in 2009 [17], while the rate constants from Antonov et al. [39] lie between them. As Antonov et al. [39] only performed their experiments in the temperature range of 400–800 K, a comparison of these rate constants at higher temperatures is also shown in Fig. 2. It is observed that the differences in all of these rate constants are within a factor of two at 1000 K. It is suggested that the reaction of $\dot{\text{O}}\text{H}$ addition to the double bond is only important at temperatures lower than 800 K. In this work, rate constants from the Antonov et al. study [39] were employed for $\dot{\text{O}}\text{H}$ addition to the central carbon site for both 1 and 2-pentene. The branching ratio of $\dot{\text{O}}\text{H}$ addition to the terminal and central carbon sites for propene is about 50:50, as

pointed out by Loison et al. [46] and Feltham et al. [47], which is consistent with the results from [17,45], while for 1-butene it is suggested to be 75:25 [46,47]. Thus, in this study, a branching ratio of 75:25 for $\dot{\text{O}}\text{H}$ addition to the terminal and central carbon sites for 1-pentene is used.

3.1.2. Waddington mechanism, hydroxy-alkylperoxy radical reactions

As suggested by Zhou et al. [44], after the addition of $\dot{\text{O}}\text{H}$ radicals to the $\text{C}=\text{C}$ double bond and the subsequent hydroxyalkyl-peroxy radical addition to O_2 , in addition to the Waddington reaction pathway, hydroxyalkyl-peroxy radicals can also isomerize via internal hydrogen atom transfer, which is similar to the low temperature chemistry of alkanes, and can ultimately contribute to low-temperature reactivity. In this work, these reactions have been added to the mechanism.

Following $\dot{\text{O}}\text{H}$ addition to the double bond, the hydroxyalkyl radicals so formed add to molecular oxygen, and the resulting hydroxy-alkylperoxy radicals can proceed through Waddington mechanism and alternate internal H-atom isomerization reactions in chain branching, similar to those for alkanes. The rate constants for the Waddington mechanism, $\text{H}\dot{\text{O}}_2$ elimination, H-shift and cyclic ether formation are taken from Lizardo-Huerta et al. [14]. For the β -scission of the hydroperoxy-alkyl oxide, other possible reaction pathways besides Waddington mechanism have also been considered, and the rate constants are taken by analogy with alkyl oxides [48].

3.1.3. Alkene + $\text{H}\dot{\text{O}}_2$ reactions

There are several reaction pathways for alkene + $\text{H}\dot{\text{O}}_2$, including H-atom abstraction by and addition of $\text{H}\dot{\text{O}}_2$ radicals to the double bond, forming alkyl-peroxy or hydroperoxy-alkyl radicals. For H-atom abstraction, rate constants are taken from Zádor et al. [18]. $\text{H}\dot{\text{O}}_2$ elimination from alkyl-peroxy or hydroperoxy-alkyl radicals is a prominent reaction pathway for alkene consumption and is also important for the corresponding saturated alkane chemistry. In previous studies of alkane chemistry oxidation [21,49,50,51], consistent rate constants were used for the same low-temperature reaction classes of different alkanes, resulting in good predictions of experimental IDT and species profile measurements. Rate constants for $\text{R}\dot{\text{O}}_2$ isomerization to $\text{Q}\dot{\text{O}}\text{OH}$ are from Sharma et al. [52], and rate constants for $\text{H}\dot{\text{O}}_2$ elimination from $\text{R}\dot{\text{O}}_2$, cyclic ether formation from $\text{Q}\dot{\text{O}}\text{OH}$ and $\text{H}\dot{\text{O}}_2$ elimination from $\text{Q}\dot{\text{O}}\text{OH}$ are from Villano et al. [53,54]. In previous studies [6,21], alkane and alkene chemistry have not been simultaneously validated. However, alkene chemistry can show different sensitivities to these important reaction classes compared to alkanes, since the reaction starts from the alkene + $\text{H}\dot{\text{O}}_2$ side in alkenes [18]. The competition of $\text{R}\dot{\text{O}}_2$ isomerization to $\text{Q}\dot{\text{O}}\text{OH}$ and $\text{H}\dot{\text{O}}_2$ elimination from $\text{R}\dot{\text{O}}_2$ is very important in predicting NTC behavior in alkanes. Among these reactions, $\text{H}\dot{\text{O}}_2$ elimination from $\text{Q}\dot{\text{O}}\text{OH}$ is more important in alkene chemistry. In this paper, the rate constants for this reaction class are taken from Zádor et al. [18]. For the reaction of $\dot{\text{C}}_5\text{H}_{10}\text{OOH1}-2$ decomposing to $\text{C}_5\text{H}_{10}-1$ and $\text{H}\dot{\text{O}}_2$, the rate constants from Zádor et al. [18] are between a factor of 9 and 3 slower than those of Villano et al. [54] at low temperatures (650–1000 K), corresponding to a difference of ~ 2 kcal mol $^{-1}$ in activation energy in the calculations performed by Zádor et al. [18] and Villano et al. [53,54].

3.1.4. H-atom abstraction reactions

In this study, H-atom abstractions by $\dot{\text{O}}$ and $\dot{\text{H}}$ atoms, and $\dot{\text{O}}\text{H}$, $\text{H}\dot{\text{O}}_2$, $\dot{\text{C}}\text{H}_3$, $\text{CH}_3\dot{\text{O}}$ and $\text{CH}_3\dot{\text{O}}_2$ radicals as well as O_2 have been considered. For H-atom abstraction by radicals, the vinylic and allylic sites are treated separately as their corresponding C–H bond dissociation energies are quite different to those for alkanes. Most of the rate constants for vinyl and allylic sites are taken by analogy

with ethylene, propene and butene which we have published previously [11,44]. For secondary and primary alkane-like carbon sites, rate constants are taken by analogy with alkane chemistry [21]. Among these reactions, H-atom abstraction by $\dot{\text{O}}\text{H}$ has the largest effect on IDT predictions.

Allylic H-atom abstraction by molecular oxygen has proven to be very important for alkene chemistry, which can inhibit fuel reactivity at low temperatures and promote fuel reactivity at high temperatures [11]. In this paper, the rate constants calculated by Zhou et al. [55] have been used for allylic H-atom abstractions by O_2 .

In addition, H-atom abstraction reactions from vinylic carbons have been adopted with rate constants from analogous reactions of the butene isomers [11,56]. Although these reactions have minor contribution to fuel consumption, their roles are not trivial, since the reaction of vinylic radicals with O_2 can greatly promote reactivity especially at high temperatures [44,57].

3.1.5. Allylic radicals + HO_2 reactions

During pentene oxidation, allylic radicals ($\dot{\text{C}}_5\text{H}_9\text{1-3}$ and $\dot{\text{C}}_5\text{H}_9\text{2-4}$) are present in much higher concentrations than other alkenyl radicals, which is due to their more favored formation channels and lower rates of consumption as they are resonantly stabilized radicals. These allylic radicals can react with HO_2 and produce $\dot{\text{O}}\text{H}$ radicals, which increases reactivity. Thus, this reaction class is very important at low to intermediate temperatures (600–900 K). The rate constants of this reaction class are based on analogy with allyl + HO_2 calculated by Goldsmith et al. [58] and the rate constants of secondary allylic radicals were increased by a factor of 2.0.

3.1.6. Alkenyl-peroxy radical (RO_2) reactions

For alkenyl-peroxy radicals, reaction pathways of HO_2 elimination, isomerization to QOOH and cycloadditions have been included in this study, with their rate constants taken from [15] and [16].

Among the alkenyl-peroxy radicals, allyl-peroxyl radicals are thermodynamically less stable than alkyl-peroxyl radicals. There are several studies of allylic RO_2 reaction pathways [15,59], however, the chemistry of allyl-peroxyl radicals are not well understood. Allylic RO_2 radical chemistry is highly dependent on the energy barriers for their stabilization in the $\text{R} + \text{O}_2 \leftrightarrow \text{RO}_2$ equilibrium, as it is very easy for them to decompose back to reactants due to the 15 kcal mol⁻¹ lower energy barrier, it being 19.9 kcal mol⁻¹ as compared to ~35 kcal mol⁻¹ for alkanes [11]. The increased carbon chain length can introduce more internal H-shift reaction pathways with lower energy barrier. For instance, when abstracting hydrogen atoms from the secondary carbon site, the energy barrier of a 1,5 H-shift reaction is comparable to that of the decomposition reaction of allylic RO_2 radicals [15]. This suggests that the allylic RO_2 reaction pathway may be important for an alkene molecule larger than 1-pentene. Also, the thermochemistry of allyl-peroxy radicals can also greatly affect the reaction pathway of allylic RO_2 radicals since it affects the reverse rate constant when only the forward rate constant is specified. The thermochemistry of $\text{C}_4\text{H}_7\text{1-3OOH}$ has been estimated using quantum chemistry calculations and also compared to values in the literature [60]. These values have been used to update the group values in the THERM code [40] to estimate the thermochemistry of larger molecules.

For non-allylic allyl-peroxyl radicals, the weaker allylic C – H bond can significantly affect the reaction pathways of RO_2 and QOOH , which will be discussed in detail in the following section.

Alkenyl-peroxy radicals can also undergo cycloaddition reactions producing cyclo-peroxy radicals. Among the three reaction pathways of alkenyl-peroxy radicals, the cycloaddition reactions may be the dominant pathways for some alkenyl-peroxy radicals,

which is mainly due to the presence of the C = C double bond which increases the energy barrier for the reactions leading to HO_2 elimination and isomerization to QOOH . This reaction pathway has been discussed previously and its importance has been highlighted [15,16,61]. More details on the cycloaddition reactions are provided in Section 4.4.

3.2. High-temperature chemistry

3.2.1. Unimolecular fuel decomposition

Unimolecular fuel decomposition reactions are very important at high temperatures. The unimolecular decomposition of 1-pentene producing allyl and ethyl radicals is one of the major reaction pathways at high temperatures (> 1200 K), which increases the system's reactivity. In addition, the retro-ene reaction producing propene and ethylene was also included. The rate constants for both reactions were measured by Tsang et al. [62] and have been adopted in this study.

3.2.2. $\dot{\text{H}}$ atom addition to the double bond

In addition to abstraction reactions by $\dot{\text{H}}$ atoms which occur at both low and high temperatures, $\dot{\text{H}}$ atom addition to the double bond producing alkyl radicals is more important at high temperatures. The rate constants for $\dot{\text{H}}$ atom addition reactions and the subsequent alkyl radical β -scission reactions are taken from the calculations by Power et al. [19].

3.2.3. Vinylic radical reactions

As discussed above, the reaction of vinylic radicals with O_2 can greatly promote reactivity, especially at high temperatures [44,57]. In this study, the rate constants of these reactions are taken by analogy with vinyl and methyl vinyl radicals from Goldsmith et al. [63] and Chen and Goldsmith [64].

3.2.4. Alkenyl radical reactions

Both isomerization and β -scission reactions of alkenyl radicals have been included with the rate constants taken from the work of Sun et al. [20].

4. Results and discussion

4.1. Model performance against experimental IDT data

Simulations of IDTs measured in both the HPST and in the RCM were performed using Chemkin software [65]. The HPST data are simulated assuming constant volume conditions. For the RCM simulations, effective volume history profiles derived from the non-reactive pressure traces were used to account for volume change and heat losses (i.e., the facility effects of the RCM).

Figures 3 and 4 show comparisons between simulated and experimental results for 1-pentene using the newly developed model. In the intermediate temperature range, the current model is slightly slow for 1-pentene at fuel-lean conditions. In the experiments, an obvious two-stage ignition behavior is only observed at low pressures for fuel-lean conditions, and the pressure rise after the first-stage ignition is very weak at high temperatures. The current model over-predicts first-stage IDTs at both 15 and 30 atm. Overall, the new model captures well the auto-ignition behavior of 1-pentene from low to high temperatures at different equivalence ratios and pressures. 1-pentene shows a less pronounced NTC behavior compared to *n*-alkanes in the intermediate temperature regime (~750–850 K). At all equivalence ratios fuel reactivity increases with increasing pressure. Moreover, it can be seen that pressure has a larger effect on observed IDTs for fuel-lean mixtures compared to fuel-rich ones, especially in the temperature range

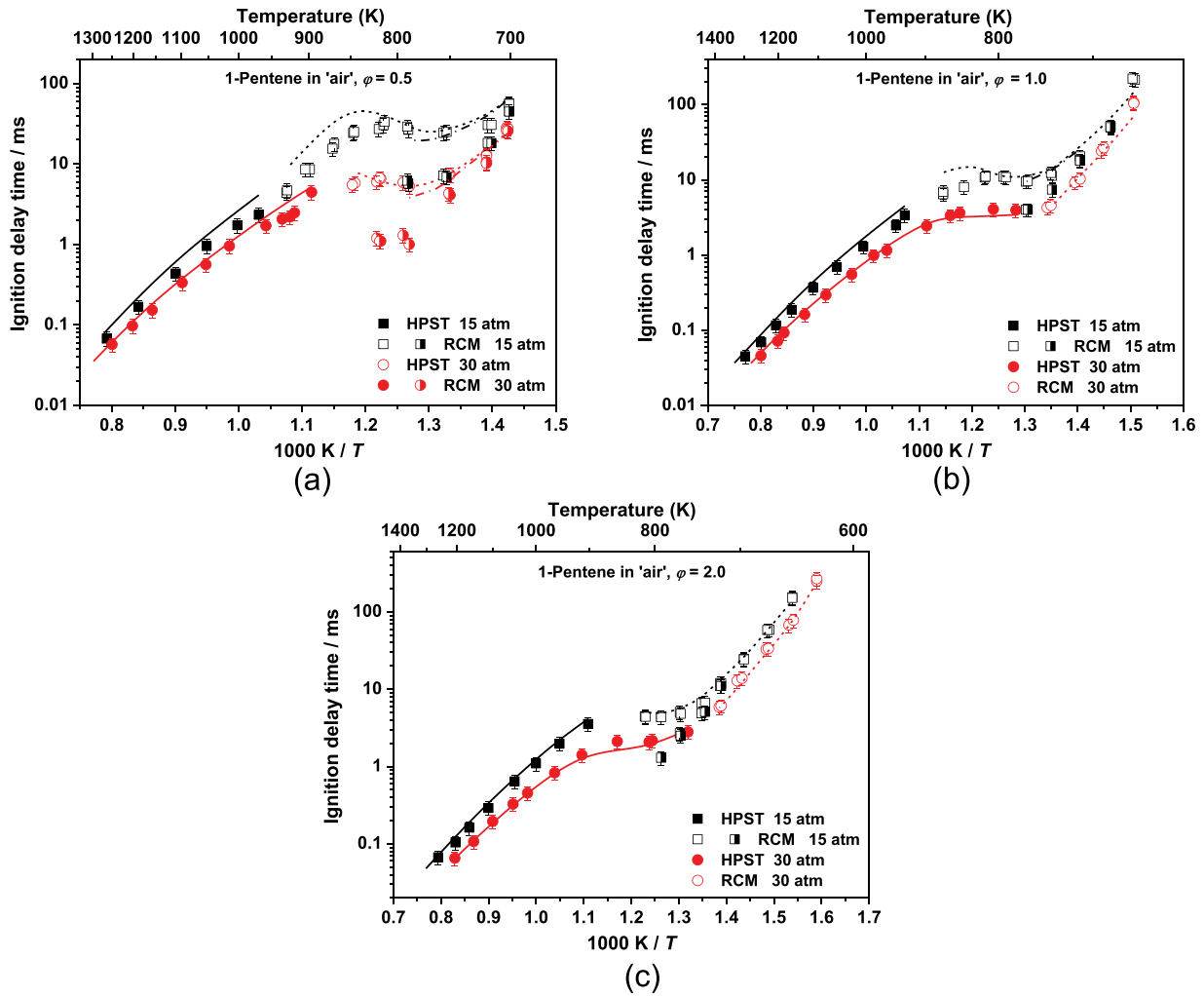


Fig. 3. Effects of pressures on 1-pentene IDTs. (a) $\phi = 0.5$, (b) $\phi = 1.0$, (c) $\phi = 2.0$. Solid symbols: HPST data. Open symbols: RCM data. Half-filled symbols: first-stage IDT data. Solid lines: constant-volume simulations. Dashed lines: RCM simulations including facility effect. Dash dotted lines: first-stage IDTs predicted for RCM simulations.

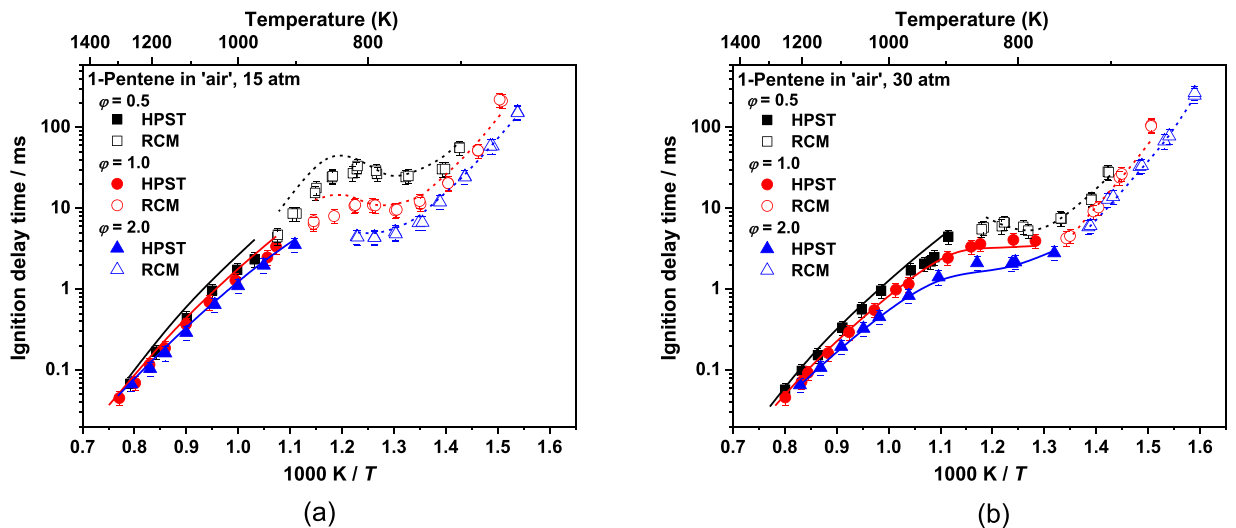


Fig. 4. Effects of equivalence ratios on 1-pentene IDTs. (a) 15 atm, (b) 30 atm. Solid symbols: HPST data. Open symbols: RCM data. Solid lines: constant-volume simulations. Dashed lines: RCM simulations including facility effect.

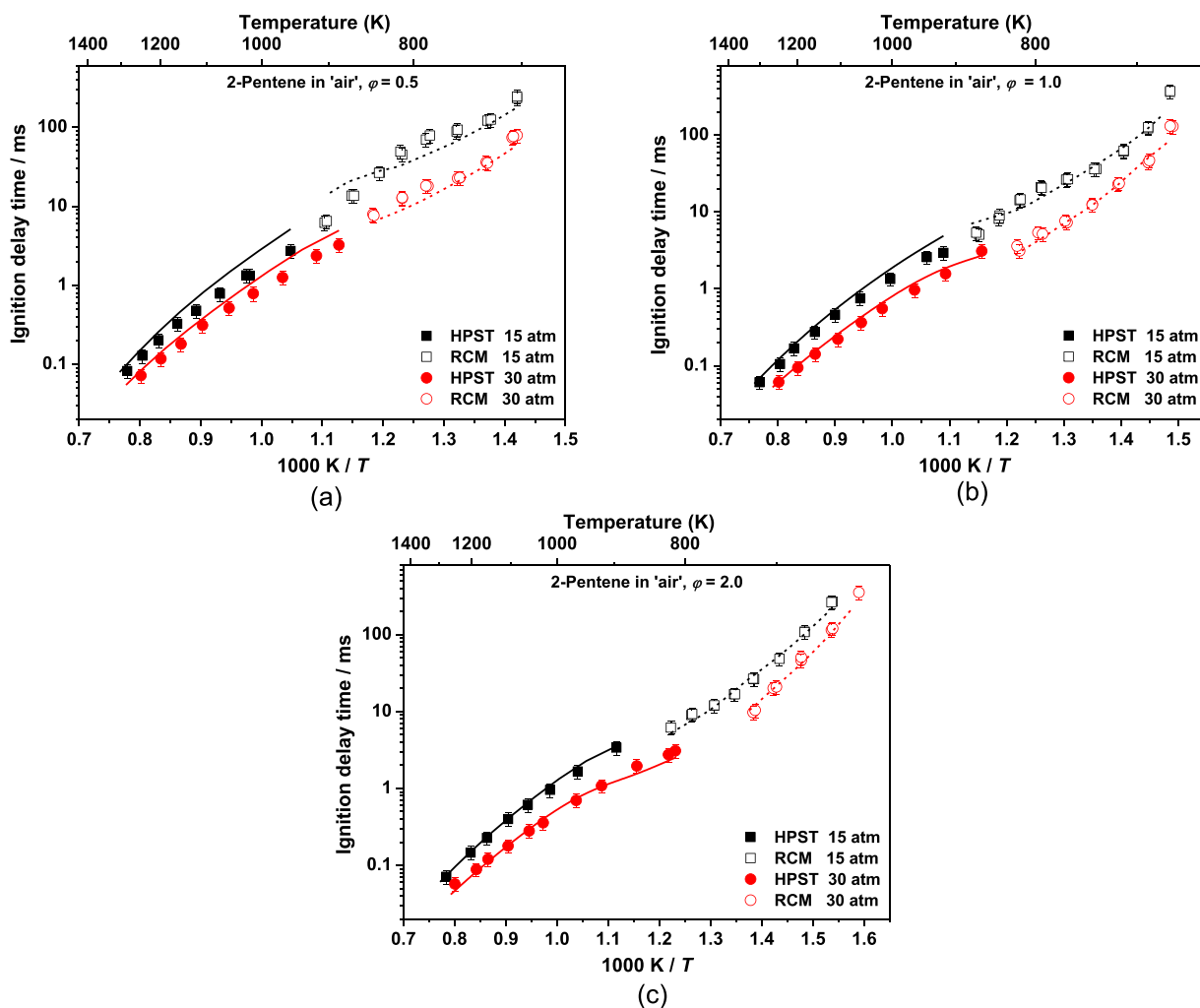


Fig. 5. Effects of pressures on 2-pentene IDTs. (a) $\phi = 0.5$, (b) $\phi = 1.0$, (c) $\phi = 2.0$. Solid symbols: HPST data. Open symbols: RCM data. Solid lines: constant-volume simulations. Dashed lines: RCM simulations including facility effect.

700–900 K (depending on the pressure), which is different compared to that for *n*-pentane [21]. This is believed due to the difference between alkane and alkene chemistry and will be discussed in detail in Section 4.4.

Figure 4 shows the equivalence ratio effects at different pressures. IDTs decrease with increasing equivalence ratios, and the model captures this effect well. Moreover, the effect of equivalence ratio on fuel reactivity decreases with increasing pressure, which is similar to the effect of pressure and will be discussed below.

Figures 5 and 6 show comparisons between simulations and experimental results for 2-pentene. 2-pentene does not show an NTC behavior, which was observed for 1-pentene. The fuel reactivity of 2-pentene increases with increasing equivalence ratios and pressures. The model captures well the experimental auto-ignition behavior of 2-pentene from low to high temperatures at different equivalence ratios and at different pressures.

Figure 7 provides a direct comparison of the reactivities of 1- and 2-pentene at 15 atm over a wide range of temperature at different equivalence ratios. Both 1- and 2-pentene show very similar reactivities at high temperatures (> 900 K). However, 1-pentene shows an NTC behavior and higher reactivity compared to 2-pentene at low- to intermediate-temperatures (~650–800 K) at different equivalence ratios. In some previous gasoline surrogate fuel models, both 1- and 2-pentene were employed to represent the alkene component [1–5]. Since the experimental re-

sults show that the low-temperature fuel reactivity of 1- and 2-pentene are different, this difference should be considered when choosing the representative components for gasoline surrogate models.

4.2. Model performance against shock-tube CO time-histories

Figures 8 and 9 show comparisons of simulated and experimental CO time-histories and IDTs for 1- and 2-pentene. Only validations of one case for each fuel are given here and all of the validation results are provided in Figs. S4 and S5 of the Supplementary material. All of these experiments were taken at highly diluted conditions, with fuel concentration of 0.25%. As can be seen, the new model slightly over-predicts the IDTs at different temperatures and the predicted position of the peak value for the CO mole fraction is also retarded. For all of the cases, auto-ignition occurs when the CO mole fraction reaches ~6000 ppm. This is mainly due to the following: both CO and $\dot{O}H$ radicals are important indicators of high temperature heat release. CO can react with hydroxyl radicals producing CO_2 and \dot{H} atoms, which results significant heat release, eventually contributing to auto-ignition. Since the reactions controlling the formation and consumption of CO are mainly included in the base chemistry, the model performance also indicates that the current base chemistry is reliable.

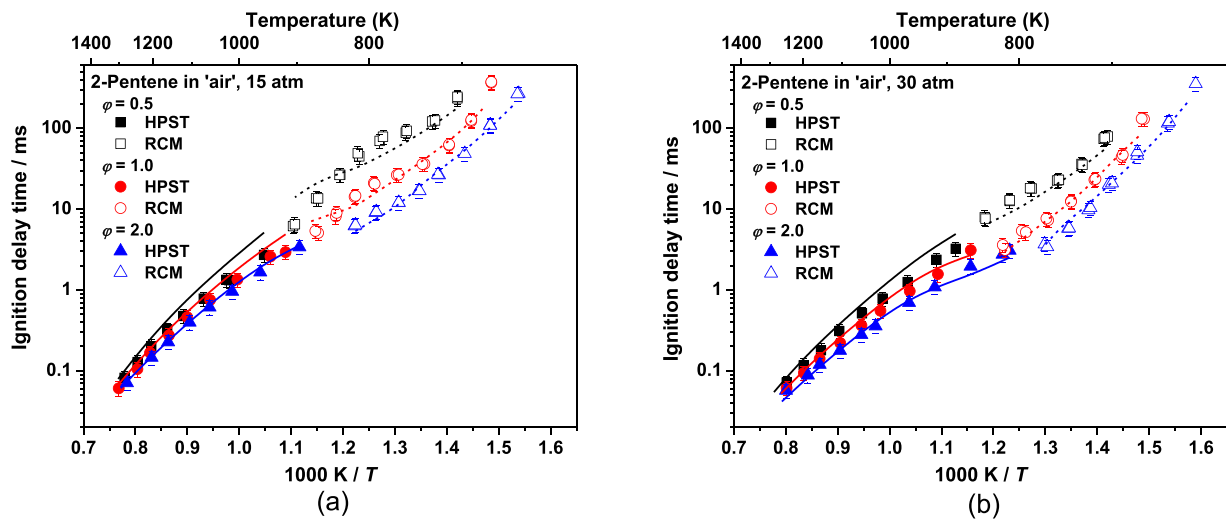


Fig. 6. Effects of equivalence ratios on 2-pentene IDTs. (a) 15 atm, (b) 30 atm. Solid symbols: HPST data. Open symbols: RCM data. Solid lines: constant-volume simulations. Dashed lines: RCM simulations including facility effects.

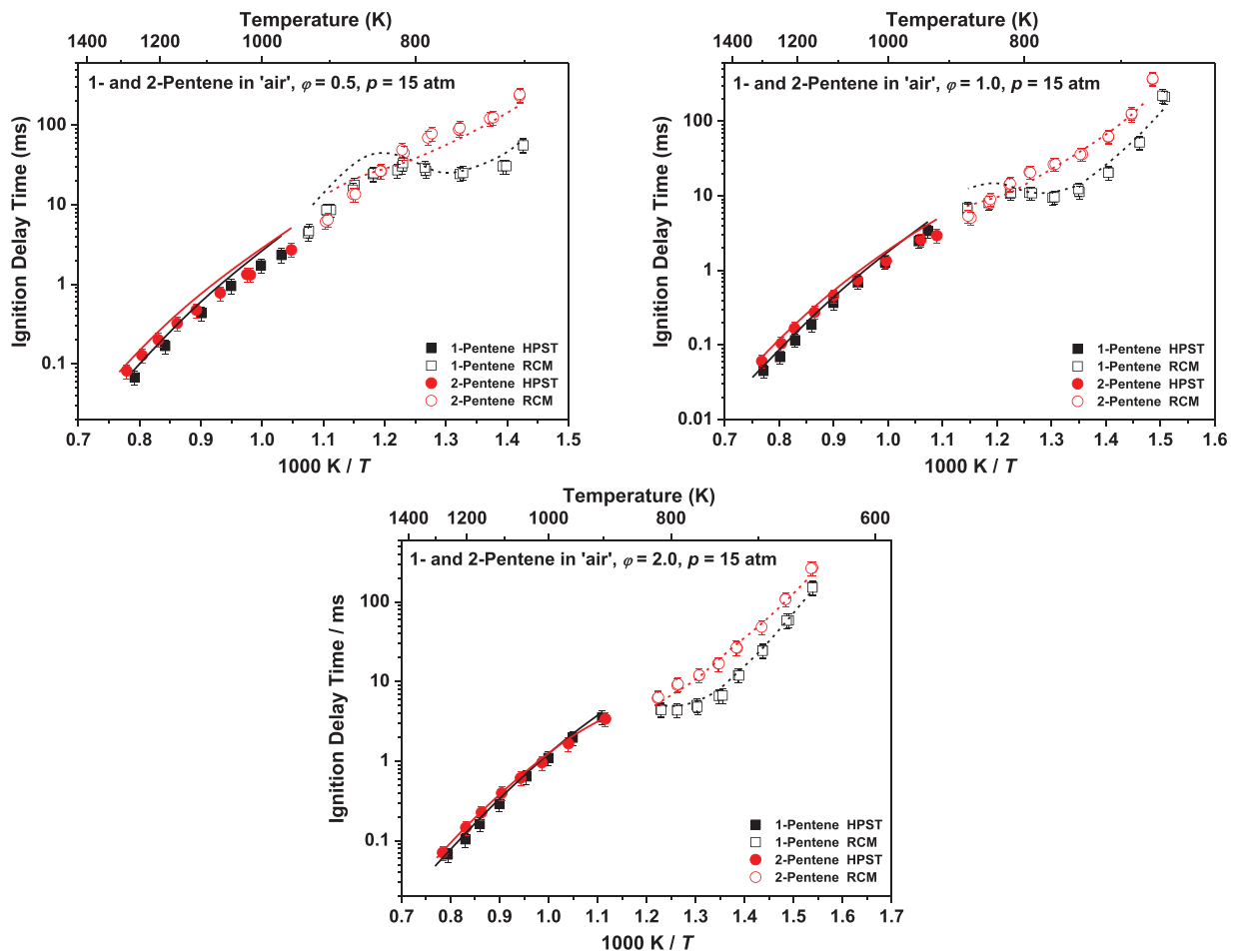


Fig. 7. Fuel reactivity comparison of 1- and 2-pentene under different pressures. Solid symbols: HPST data. Open symbols: RCM data. Solid lines: constant-volume simulations. Dashed lines: RCM simulations including facility effect.

4.3. Model performance against experimental JSR data

Figure 10 shows comparisons of simulated and experimental JSR species profiles for 1- and 2-pentene. Only validations for important species are given here and all of the validation results are given in Fig. S7 of the Supplementary material. The current

model over-predicts the CO_2 mole fraction for 1-pentene at 1025 K, which may be attributed to the high concentration of C_2 species (acetylene and ethylene) in the experiments at the same condition. The model predicts that these species are oxidized at 1025 K, while in the experiments this oxidation may be shifted to slightly

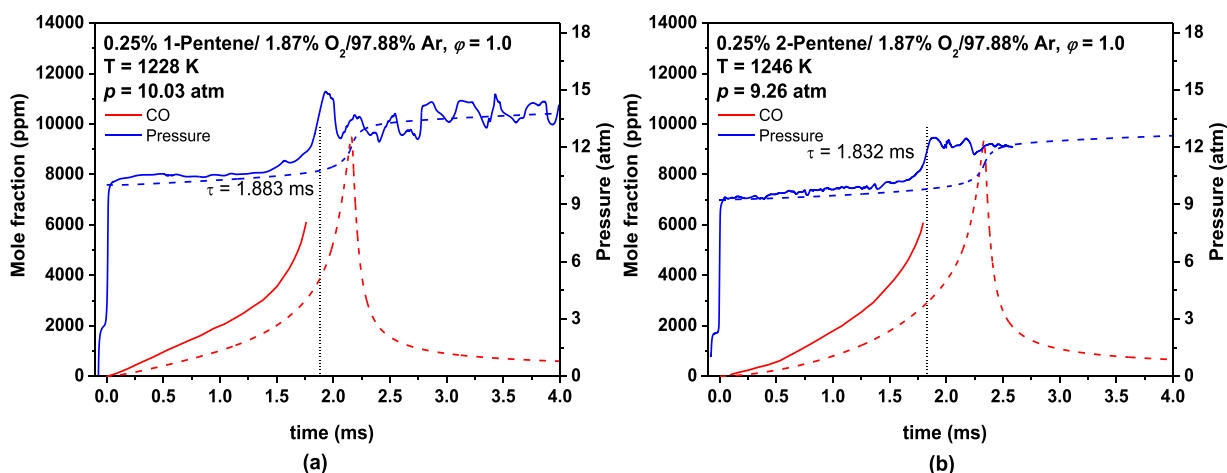


Fig. 8. Pressure (blue) and carbon monoxide time-histories (red) during oxidation ($\varphi = 1$): (a) 1-pentene at $T = 1228\text{ K}$, $p = 10.03\text{ atm}$, (b) 2-pentene at $T = 1246\text{ K}$, $p = 9.26\text{ atm}$. Solid lines represent experimental results and dashed lines the mechanism simulations. (For interpretation of the references to color in this figure legend, the reader is referred to the web version of this article.)

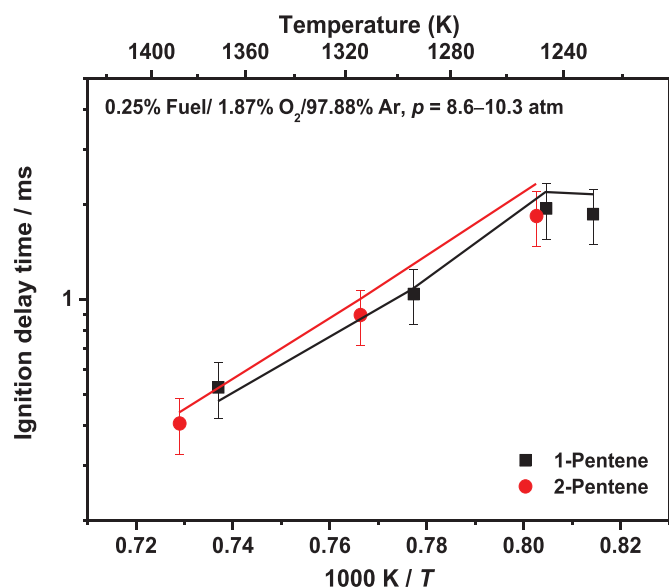


Fig. 9. Ignition delay time of stoichiometric oxidation of 1 and 2-pentene in oxygen, (0.25% fuel loading, balanced in argon). IDTs are defined as the maximum pressure rise rate due to ignition. Solid symbols: experimental data. Solid lines: simulations including pressure rise.

higher temperatures not measured here. Overall, the newly developed model can capture well most of the species profiles.

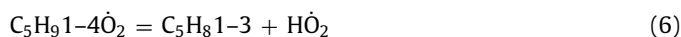
In this study, new IDT data, CO time histories and species profiles were measured at different conditions, for fuel in 'air' and highly diluted conditions, in various facilities. The newly developed model can capture well all of these targets.

4.4. Flux and sensitivity analyses based on the newly developed model

To better understand the difference in reactivity of both fuels, flux and sensitivity analyses were performed using the Chemkin [65] software. Figure 11 shows the flux analyses results for both 1- and 2-pentene, with only the major reaction pathways shown.

At 650 K, more than 96% of 1- and 2-pentene are consumed via reaction with hydroxyl radicals. About 33% of the fuel molecules

are consumed via H-atom abstraction by $\dot{\text{O}}\text{H}$ radicals, and the remaining 63% of the fuel is consumed by addition of $\dot{\text{O}}\text{H}$ radicals to the double bond. H-atom abstraction leading to the formation of three different pentenyl radicals, with 1-penten-3-yl ($\dot{\text{C}}_5\text{H}_9\text{1-3}$) being the major radical formed (19.9%) as it is resonantly stabilized. Most of these react with $\text{H}\dot{\text{O}}_2$ and ultimately produce $\text{C}_5\text{H}_9\text{O1-3}$ / $\text{C}_5\text{H}_9\text{O2-1}$ and $\dot{\text{O}}\text{H}$ radicals. The subsequent decomposition of $\text{C}_5\text{H}_9\text{O1-3}$ radicals mainly produces ethyl radicals and acrolein. The other two pentenyl radicals, 1-penten-4-yl ($\dot{\text{C}}_5\text{H}_9\text{1-4}$) and 1-penten-5-yl ($\dot{\text{C}}_5\text{H}_9\text{1-5}$) mainly add to O_2 to form alkenyl-peroxy radicals.



About 51% of $\text{C}_5\text{H}_9\text{1-4}\dot{\text{O}}_2$ radicals are consumed via concerted $\text{H}\dot{\text{O}}_2$ elimination producing 1,3-pentadiene ($1,3\text{-C}_5\text{H}_8$) + $\text{H}\dot{\text{O}}_2$ as the C-H bond of the allylic site is weaker and a five-membered transition state (TS) ring H-atom isomerization reaction is involved, Eqs. (5) and (6) and another major reaction pathway (~40%) is cycloaddition. $\text{C}_5\text{H}_9\text{1-5}\dot{\text{O}}_2$ radicals mainly undergo isomerization to hydroperoxy-alkenyl radicals followed by a second addition to O_2 leading to chain branching, as this sequence involves six-membered TS ring isomerization reactions, Eqs. (7) and (8). Therefore, for the reaction pathways of pentenyl radicals, reactive hydroxyl radicals are consumed by H-atom abstraction reactions while fewer of them or less reactive hydroperoxyl radicals are produced due to the presence of the double bond in 1-pentene relative to *n*-pentane, thus decreasing the reactivity of 1-pentene relative to *n*-pentane. For 2-pentene, approximately 42% of fuel molecules are consumed through H-atom abstraction, with 1-penten-3-yl ($\dot{\text{C}}_5\text{H}_9\text{1-3}$) and 1-penten-4-yl ($\dot{\text{C}}_5\text{H}_9\text{2-4}$) being the major radicals formed as they are resonantly stabilized, and the subsequent reaction pathways of these pentenyl radicals are similar to those in 1-pentene. $\text{C}_5\text{H}_9\text{2-5}\dot{\text{O}}_2$ radicals mainly undergo cycloaddition reactions producing cyclo-peroxy radicals, which indicates cycloaddition should be included in the low-temperature mechanisms of alkenes.

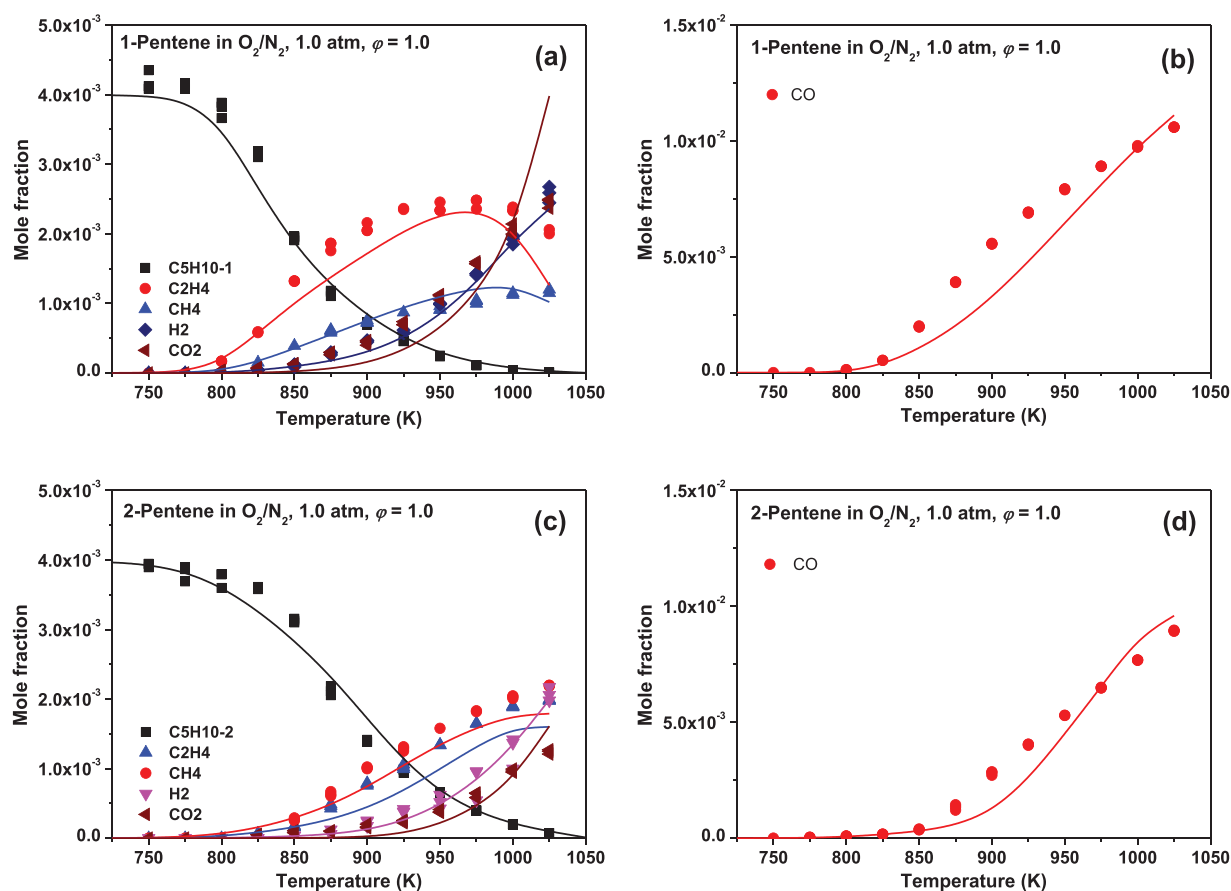


Fig. 10. Experimental and simulated results of species data. Solid symbols: JSR data. Solid lines: model simulations.

Approximately 63% of 1-pentene is consumed via the Waddington mechanism in which hydroxyl radicals add across the double bond, leading to the formation of $\dot{C}_5H_{10}OH1-2$ and $\dot{C}_5H_{10}OH2-1$ radicals. These radicals then add to molecular oxygen to produce $C_5H_{10}OH1-2O_2$ and $\dot{C}_5H_{10}OH2-1O_2$ radicals and can subsequently react by abstracting the alkoxy H-atom with subsequent decomposition of the hydroperoxy-alkoxy radical producing aldehydes and $\dot{O}H$ radicals. However, in addition to this Waddington reaction pathway, $C_5H_{10}OH1-2O_2$ and $\dot{C}_5H_{10}OH2-1O_2$ radicals can also undergo internal H-atom re-arrangements of available H-atoms on other carbon sites to form alcoholic hydroperoxyl-alkyl radicals which can add to O_2 and proceed to chain branching. For 1-pentene, almost 19% of the fuel flux proceeds via this chain branching pathway. Therefore, for 1-pentene, the $C_5H_{10}OH1-2O_2$ and $C_5H_{10}OH2-1O_2$ radicals and $C_5H_91-5\dot{O}_2$ radical contribute to chain branching reaction pathways, with the $C_5H_{10}OH1-2O_2$ radical contributing most. However, for 2-pentene fewer fuel molecules (45%) go through the Waddington mechanism as the rate of $\dot{O}H$ radical addition to the central carbon site is slower than that to the terminal carbon site. Moreover, due to the location of the hydroxyl group, H-atom transfer from the carbon site with the hydroxyl group is the dominant reaction pathway other than H-atom transfer from the primary carbon sites, due to the weaker C–H bond resulting from the hydroxyl group. Therefore, the radicals formed by $\dot{O}H$ addition across the double bond mainly decompose via chain propagation reaction pathways. As a result, 2-pentene shows lower fuel reactivity compared to 1-pentene at low-temperatures.

At 800 K, as can be seen from Fig. 11, the branching ratio of $\dot{O}H$ radicals adding to the double bond decreases for both 1- and

2-pentene, which is mainly due to the competition with H-atom abstraction by $\dot{O}H$ radicals. As shown in Fig. 3, in this temperature regime, a less pronounced NTC behavior is observed for 1-pentene compared to *n*-pentane. The NTC behavior observed in *n*-alkanes is believed to be mainly due to the competition of chain branching and chain propagation reaction pathways [21], with the chain propagation pathway mainly producing $\dot{H}O_2$ radicals, which decreases the system's reactivity and consequently results in a more pronounced NTC behavior. However, for 1-pentene, both the reaction pathways of H-atom abstraction producing alkenyl radicals and the Waddington mechanism compete with the chain branching reaction pathways. Both the Waddington mechanism and the reaction pathway of 1-penten-3-yl radicals with $\dot{H}O_2$ produce reactive $\dot{O}H$ radicals rather than less reactive $\dot{H}O_2$ radicals which are produced from alkyl-peroxy radical elimination reactions or alkyl radicals produced from β -scission of alkyl radicals in alkanes. As the chain propagation reaction mainly produces reactive $\dot{O}H$ radicals rather than $\dot{H}O_2$ radicals, the competition of chain propagation and chain branching reaction pathways shows a relatively smaller effect on auto-ignition for alkenes compared to alkanes. Therefore, a less pronounced NTC behavior is observed for 1-pentene.

As discussed in Section 4.1, the effect of increasing pressure decreases as the fuel mixtures become richer, which is different to that observed for *n*-pentane [21]. For alkane chemistry, in the intermediate temperature regime, an increase in fuel reactivity with increasing pressure is mainly due to the chain branching pathways: $RH + \dot{H}O_2 = \dot{R} + H_2O_2$ followed by $H_2O_2 (+M) = \dot{O}H + \dot{O}H (+M)$, since the fuel concentration ($[RH]$) increases with increasing pressure. Therefore, increasing fuel reactivity with increasing

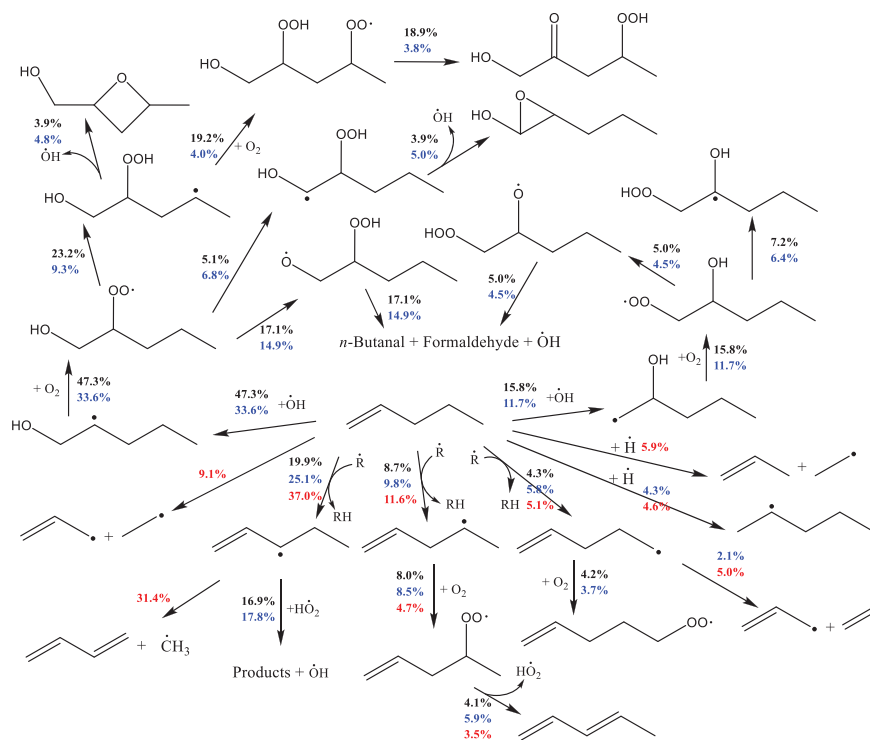
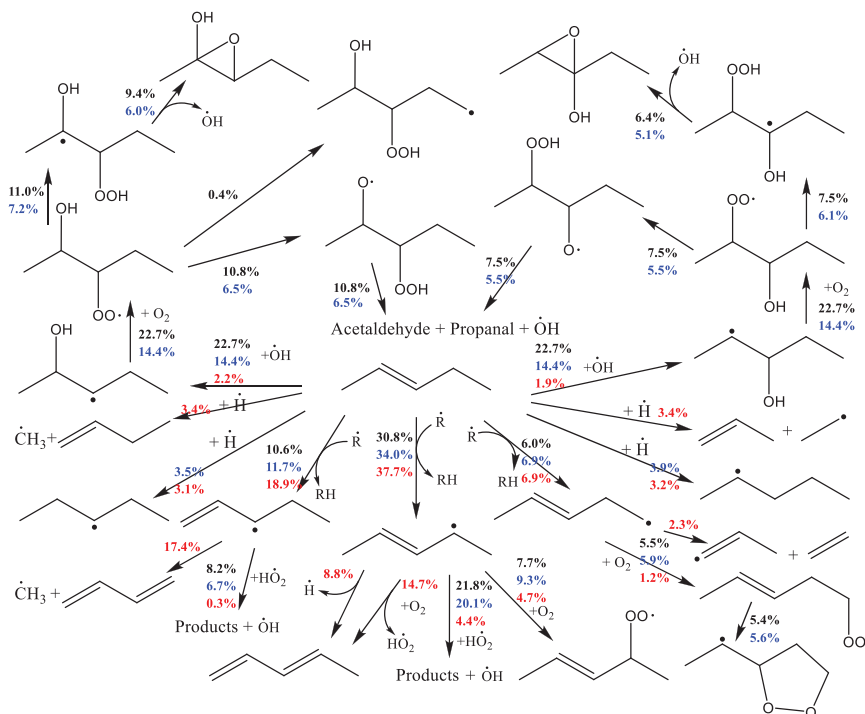
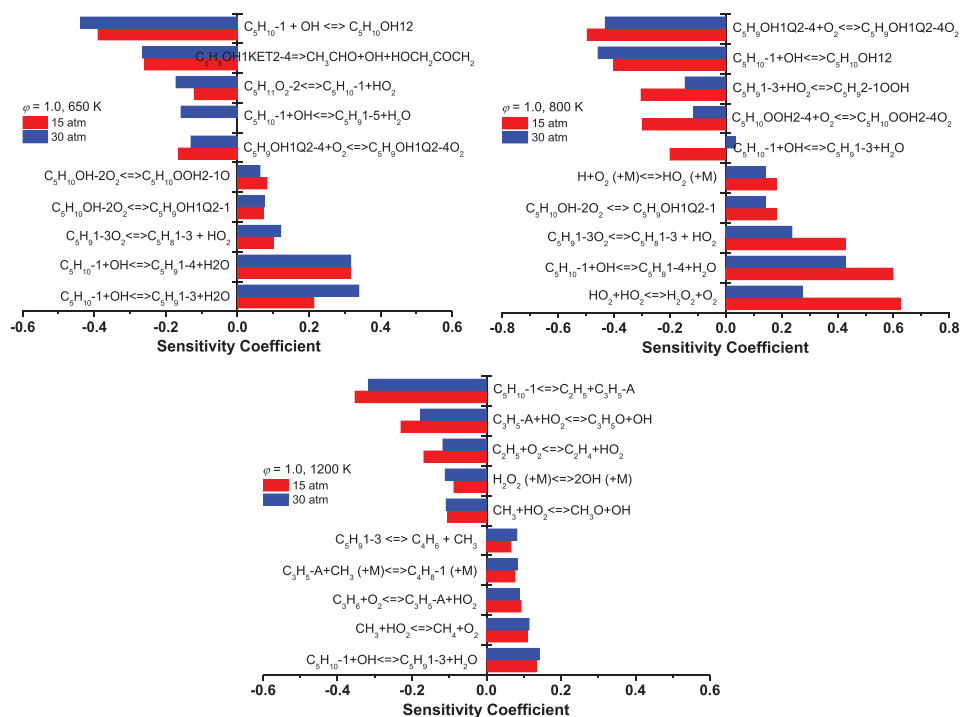
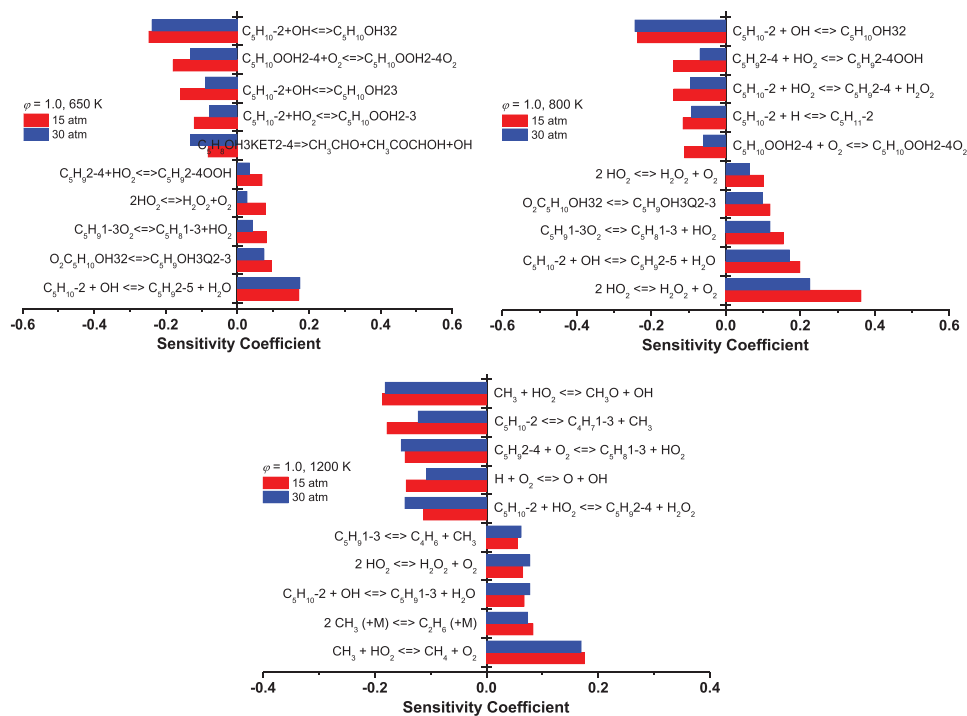
(a) C_5H_{10-1} (b) C_5H_{10-2}

Fig. 11. Flux analysis results based on constant volume simulations for 1- and 2-pentene at $\phi = 1.0$ in 'air', $p = 30$ atm and 20% fuel consumed. Numbers represent the percentage of fuel flux that goes into a particular species. Black numbers represent flux at 650 K, blue numbers represent flux at 800 K, and red numbers represent flux at 1200 K. \dot{R} is the sum of $\dot{O}H$, \dot{H}_2O_2 and $\dot{C}H_3$ radicals and \dot{H} and \dot{O} atoms. (For interpretation of the references to color in this figure legend, the reader is referred to the web version of this article.)



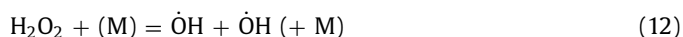
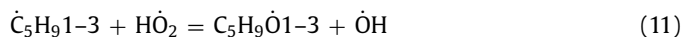
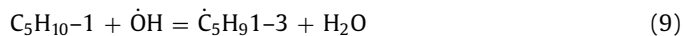
(a) C₅H₁₀-1



(b) C₅H₁₀-2

Fig. 12. Sensitivity analyses for 1- and 2-pentene at $\phi = 1.0$ in 'air', $p = 15$ and 30 atm, and $T = 650, 800, 1200$ K.

pressure does not change much at different equivalence ratios. However, for 1-pentene, in this temperature regime, 1-penten-3-yl (\dot{C}_5H_91-3) radicals mainly react with $\dot{H}O_2$ producing $\dot{C}_5H_9\dot{O}1-3$ radical and one $\dot{O}H$ radical. With increasing equivalence ratios, the increased fuel concentration ($[RH]$) results in higher concentrations of \dot{C}_5H_91-3 radicals and promotes the reaction of \dot{C}_5H_91-3 with $\dot{H}O_2$ radicals. Consequently, this results in fewer $\dot{H}O_2$ re-combinations producing H_2O_2 which decomposes into two $\dot{O}H$ radicals, Eqs. (9)–(12).



Flux analysis results for $\dot{H}O_2$ consumption at different conditions are provided in Fig. S11 of the Supplementary material. The $\dot{H}O_2$ flux of H-atom abstraction by $\dot{H}O_2$ radicals from stable molecules does not change much at different conditions. With increasing equivalence ratios, more $\dot{H}O_2$ radicals react with \dot{C}_5H_91-3 radicals producing $\dot{O}H$ radicals, and the percentage of $\dot{H}O_2$ recombining to produce H_2O_2 decreases. In this temperature range, only 20 – 50% of H_2O_2 decomposes into two $\dot{O}H$ radicals. Thus, the reactions of 1-penten-3-yl (\dot{C}_5H_91-3) and $\dot{H}O_2$ radicals are more efficient in converting $\dot{H}O_2$ radicals into $\dot{O}H$ radicals, and hence these reaction pathways promote reactivity. At fuel-lean conditions, the fraction of $\dot{H}O_2$ radicals that react with \dot{C}_5H_91-3 radicals increases significantly as the pressure increases from 15 atm to 30 atm. For stoichiometric and fuel-rich conditions, the fraction of $\dot{H}O_2$ radicals that react with \dot{C}_5H_91-3 radicals does not change as much with increasing pressure as observed at fuel-lean conditions. That is the major reason that pressure shows a greater effect on IDTs at fuel-lean compared to fuel-rich conditions.

At 1200 K, most of 1-pentene is consumed by H-atom abstraction producing alkenyl radicals, with the Waddington mechanism no longer important. Most \dot{C}_5H_91-3 and \dot{C}_5H_91-5 radicals undergo β -scission reactions. For \dot{C}_5H_91-4 radicals, a large proportion (~54%) of these radicals undergo β -scission and isomerization reactions. About 40% of these radicals add to O_2 to form alkenyl-peroxy radicals and, following $\dot{H}O_2$ elimination, produce 1,3-pentadiene and $\dot{H}O_2$ radicals. Other important reaction pathways include unimolecular decomposition and H-atom addition to the double bond, producing smaller alkenes, and alkenyl and alkyl radicals. For 2-pentene, most of the fuel is consumed by H-atom abstraction producing alkenyl radicals. The reaction of \dot{C}_5H_91-3 radicals is similar to those of 1-pentene, producing 1,3-butadiene and $\dot{C}H_3$ radicals. \dot{C}_5H_92-4 radicals mostly undergo β -scission and/or reactions with O_2 producing 1,3-pentadiene, and most \dot{C}_5H_92-5 radicals proceed by addition to O_2 to form alkenyl-peroxy radicals followed by $\dot{H}O_2$ elimination producing 1,3-pentadiene. At high temperatures (> 1200 K), the reactivity of 2-pentene is slightly lower than that of 1-pentene, mainly because 1-pentene produces higher concentrations of smaller alkenes and alkenyl radicals which promote reactivity. However, for 2-pentene, more than 30% of the fuel is consumed by producing 1,3-pentadiene, consequently inhibiting reactivity.

Figure 12 shows the results of brute force sensitivity analyses for both 1- and 2-pentene. Positive values indicate reactions that inhibit reactivity and negative values promote reactivity. The brute force sensitivity results are consistent with, and support, the flux analysis results. For 1-pentene, the reactions that promote reactivity include hydroxyl radical addition to the double bond and the following chain branching reactions. Competing with

the reaction pathway of $\dot{O}H$ addition, reactions that consuming hydroxyl radicals and producing pentenyl radicals inhibit reactivity. For 2-pentene, the sensitivity coefficients of the reactions are much lower than those for 1-pentene. Meanwhile, the reactions associated with the Waddington mechanism have a smaller effect on reactivity compared to those for 1-pentene because the produced hydroxy-alkylperoxy radicals mainly undergo chain termination and propagation reactions.

5. Conclusions

- (1) Ignition delay times for 1- and 2-pentene oxidation in 'air' at various equivalence ratios, at 15 and 30 atm and over a wide temperature range were studied using both a high-pressure shock tube and a rapid compression machine. These new data together with species profiles measured in a JSR and CO time-histories measured in a HPST are used for model validation.
- (2) The experimental results show that 1- and 2-pentene show similar fuel reactivities at high temperatures (> 900 K), while 1-pentene shows an NTC behavior and higher fuel reactivity compared to 2-pentene at intermediate temperatures (650–800 K).
- (3) The newly developed chemical kinetic model can capture well the auto-ignition behavior of both 1- and 2-pentene at different temperatures and pressures. Flux and sensitivity analyses show that, at low temperatures, hydroxyl radicals add across the double bond, followed by addition to molecular oxygen producing hydroxy-alkylperoxy radicals. These radicals can further proceed via the Waddington mechanism or other alternate internal H-atom isomerization reactions in a chain branching mechanism similar to those for alkanes, and this chain branching reaction pathway is responsible for the higher fuel reactivity of 1-pentene relative to 2-pentene at low temperatures.
- (4) To help further validate the chemical model, a robust evaluation of low-temperature oxidation products and high-temperature pyrolysis products could be performed in the future.

Declaration of Competing Interest

The authors declare that they have no known competing financial interests or personal relationships that could have appeared to influence the work reported in this paper.

Acknowledgments

The authors at NUI Galway recognize funding support from Science Foundation Ireland (SFI) via project number 16/SP/3829 and also funding from Computational Chemistry LLC. The work at LLNL was performed under the auspices of the U.S. Department of Energy (DOE) by Lawrence Livermore National Laboratory under Contract DE-AC52-07NA27344 and was conducted as part of the Co-Optimization of Fuels & Engines (Co-Optima) project sponsored by the DOE Office of Energy Efficiency and Renewable Energy (EERE), Bioenergy Technologies and Vehicle Technologies Offices. The work at KAUST was supported by the KAUST Clean Fuels Consortium (KCFC) via its Office of Sponsored Research and member companies. This work at UCF was conducted as part of the Co-Optimization of Fuels & Engines (Co-Optima) project sponsored by the U.S. Department of Energy (DOE) Office of Energy Efficiency and Renewable Energy (EERE) [grant numbers DE-EE007982, DE-EE007984].

Disclaimer

This report was prepared as an account of work sponsored by an agency of the United States Government. Neither the United States Government nor any agency thereof, nor any of their employees, makes any warranty, express or implied, or assumes any legal liability or responsibility for the accuracy, completeness, or usefulness of any information, apparatus, product, or process disclosed, or represents that its use would not infringe privately owned rights. Reference herein to any specific commercial product, process, or service by trade name, trademark, manufacturer, or otherwise does not necessarily constitute or imply its endorsement, recommendation, or favoring by the United States Government or any agency thereof. The views and opinions of authors expressed herein do not necessarily state or reflect those of the United States Government or any agency thereof.

Supplementary materials

Supplementary material associated with this article can be found, in the online version, at doi:10.1016/j.combustflame.2020.09.012.

References

- [1] C.V. N. aik, W.J. Pitz, M. Sjöberg, J.E. Dec, J. Orme, H.J. Curran, J.M. Simmie, C.K. Westbrook, Detailed Chemical Kinetic Modelling of Surrogate Fuels for Gasoline and Application to an HCCI Engine (2005) Technical Paper.
- [2] S.M. Sarathy, A. Farooq, G.T. Kalghatgi, Recent progress in gasoline surrogate fuels, *Prog. Energy Combust. Sci.* 65 (2018) 67–108.
- [3] D.B. Lenhart, D.L. Miller, N.P. Cernansky, K.G. Owens, The oxidation of a gasoline surrogate in the negative temperature coefficient region, *Combust. Flame* 156 (2009) 549–564.
- [4] M. Mehl, J.Y. Chen, W.J. Pitz, S.M. Sarathy, C.K. Westbrook, An approach for formulating surrogates for gasoline with application toward a reduced surrogate mechanism for CFD engine modeling, *Energy Fuels* 25 (2011) 5215–5223.
- [5] G. Kukkadapu, K. Kumar, C.J. Sung, M. Mehl, W.J. Pitz, Autoignition of gasoline surrogates at low temperature combustion conditions, *Combust. Flame* 162 (2015) 2272–2285.
- [6] M. Ribaucour, R. Minetti, L.R. Sochet, Autoignition of n-pentane and 1-pentene: experimental data and kinetic modeling, *Symp. (Int.) Combust.* (1998), pp. 345–351.
- [7] S. Touchard, F. Buda, G. Dayma, P.A. Claude, R. Fournet, F. Battin-Leclerc, Experimental and modeling study of the oxidation of 1-pentene at high temperature, *Int. J. Chem. Kinet.* 37 (2005) 451–463.
- [8] M. Mehl, W.J. Pitz, C.K. Westbrook, K. Yasunaga, C. Conroy, H.J. Curran, Autoignition behavior of unsaturated hydrocarbons in the low and high temperature regions, *Proc. Combust. Inst.* 33 (2011) 201–208.
- [9] Y. Cheng, E. Hu, F. Deng, F. Yang, Y. Zhang, C. Tang, Z. Huang, Experimental and kinetic comparative study on ignition characteristics of 1-pentene and n-pentane, *Fuel* 172 (2016) 263–272.
- [10] Y. Cheng, E. Hu, X. Lu, X. Li, J. Gong, Q. Li, Z. Huang, Experimental and kinetic study of pentene isomers and n-pentane in laminar flames, *Proc. Combust. Inst.* 36 (2017) 1279–1286.
- [11] Y. Li, C.W. Zhou, H.J. Curran, An extensive experimental and modeling study of 1-butene oxidation, *Combust. Flame* 181 (2017) 198–213.
- [12] M. Mehl, G. Vanhove, W.J. Pitz, E. Ranzi, Oxidation and combustion of the n-hexene isomers: a wide range kinetic modeling study, *Combust. Flame* 155 (2008) 756–772.
- [13] Y. Wu, Y. Liu, C. Tang, Z. Huang, Ignition delay times measurement and kinetic modeling studies of 1-heptene, 2-heptene and n-heptane at low to intermediate temperatures by using a rapid compression machine, *Combust. Flame* 197 (2018) 30–40.
- [14] J.C. Lizardo-Huerta, B. Sirjean, R. Bounaceur, R. Fournet, Intramolecular effects on the kinetics of unimolecular reactions of β -HORO and HOQOOH radicals, *Phys. Chem. Chem. Phys.* 18 (2016) 12231–12251.
- [15] X. You, Y. Chi, T. He, Theoretical analysis of the effect of C=C double bonds on the low-temperature reactivity of alkenylperoxy radicals, *J. Phys. Chem. A* 120 (2016) 5969–5978.
- [16] X. Sun, W. Zong, J. Wang, Z. Li, X. Li, Pressure-dependent rate rules for cycloaddition, intramolecular H-shift, and concerted elimination reactions of alkenyl peroxy radicals at low temperature, *Phys. Chem. Chem. Phys.* (2019) 10693–10705.
- [17] J. Zádor, A.W. Jasper, J.A. Miller, The reaction between propene and hydroxyl, *Phys. Chem. Chem. Phys.* 11 (2009) 11040–11053.
- [18] J. Zádor, S.J. Klippenstein, J.A. Miller, Pressure-dependent OH yields in alkene + HO₂ reactions: a theoretical study, *J. Phys. Chem. A* 115 (2011) 10218–10225.
- [19] J. Power, K.P. Somers, C.W. Zhou, S. Peukert, H.J. Curran, Theoretical, experimental, and modeling study of the reaction of hydrogen atoms with 1- And 2-pentene, *J. Phys. Chem. A* 123 (2019) 8506–8526.
- [20] Y. Sun, C.W. Zhou, K.P. Somers, H.J. Curran, Ab initio/transition-state theory study of the reactions of C₅H₉ species of relevance to 1,3-pentadiene, part I: potential energy surfaces, thermochemistry, and high-pressure limiting rate constants, *J. Phys. Chem. A* 123 (2019) 9019–9052.
- [21] J. Bugler, B. Marks, O. Mathieu, R. Archuleta, A. Camou, C. Grégoire, K.A. Heufer, E.L. Petersen, H.J. Curran, An ignition delay time and chemical kinetic modeling study of the pentane isomers, *Combust. Flame* 163 (2016) 138–156.
- [22] D. Darcy, C.J. Tobin, K. Yasunaga, J.M. Simmie, J. Würmel, W.K. Metcalfe, T. Niass, S.S. Ahmed, C.K. Westbrook, H.J. Curran, A high pressure shock tube study of n-propylbenzene oxidation and its comparison with n-butylbenzene, *Combust. Flame* 159 (2012) 2219–2232.
- [23] D. Darcy, H. Nakamura, C.J. Tobin, M. Mehl, W.K. Metcalfe, W.J. Pitz, C.K. Westbrook, H.J. Curran, A high-pressure rapid compression machine study of n-propylbenzene ignition, *Combust. Flame* 161 (2014) 65–74.
- [24] C. Morley, *GasEq, Version 0.76*. <http://www.gaseq.co.uk>, 2004.
- [25] J. Shao, R. Choudhary, D.F. Davidson, R.K. Hanson, S. Barak, S. Vasu, Ignition delay times of methane and hydrogen highly diluted in carbon dioxide at high pressures up to 300 atm, *Proc. Combust. Inst.* 37 (2019) 4555–4562.
- [26] G. Barari, O. Pryor, B. Koroglu, S.M. Sarathy, A.E. Masunov, S.S. Vasu, High temperature shock tube experiments and kinetic modeling study of diisopropyl ketone ignition and pyrolysis, *Combust. Flame* 177 (2017) 207–218.
- [27] S. Barak, O. Pryor, J. Lopez, E. Ninnemann, S. Vasu, B. Koroglu, High-speed imaging and measurements of ignition delay times in oxy-syngas mixtures with high CO₂ dilution in a shock tube, *J. Eng. Gas Turbines Power* 139 (2017) 1–7.
- [28] B. Koroglu, S.S. Vasu, Measurements of propanal ignition delay times and species time histories using shock tube and laser absorption, *Int. J. Chem. Kinet.* 48 (2016) 679–690.
- [29] E. Ninnemann, B. Koroglu, O. Pryor, S. Barak, L. Nash, Z. Loparo, J. Sosa, K. Ahmed, S. Vasu, New insights into the shock tube ignition of H₂/O₂ at low to moderate temperatures using high-speed end-wall imaging, *Combust. Flame* 187 (2018) 11–21.
- [30] O. Pryor, S. Barak, B. Koroglu, E. Ninnemann, S.S. Vasu, Measurements and interpretation of shock tube ignition delay times in highly CO₂ diluted mixtures using multiple diagnostics, *Combust. Flame* 180 (2017) 63–76.
- [31] B. Koroglu, S.S. Vasu, Measurements of propanal ignition delay times and species time histories using shock tube and laser absorption, *Int. J. Chem. Kinet.* 48 (2016) 679–690.
- [32] S. Neupane, R.K. Rahman, J. Baker, F. Arafin, E. Ninnemann, K. Thurmond, C.H. Wang, A.E. Masunov, S.S. Vasu, DMMP pyrolysis and oxidation studies at high temperature inside a shock tube using laser absorption measurements of CO, *Combust. Flame* 214 (2020) 14–24.
- [33] A.R. Laich, E. Ninnemann, S. Neupane, R. Rahman, S. Barak, W.J. Pitz, S.S. Goldsborough, S.S. Vasu, High-pressure shock tube study of ethanol oxidation: ignition delay time and CO time-history measurements, *Combust. Flame* 212 (2020) 486–499.
- [34] X. Dong, E. Ninnemann, D.S. Ranasinghe, A. Laich, R. Greene, S.S. Vasu, W.H. Green, Revealing the critical role of radical-involved pathways in high temperature cyclopentanone pyrolysis, *Combust. Flame* 216 (2020) 280–292.
- [35] E. Ninnemann, G. Kim, A. Laich, B. Almansour, A.C. Terracciano, S. Park, K. Thurmond, S. Neupane, S. Wagnon, W.J. Pitz, S.S. Vasu, Co-optima fuels combustion: a comprehensive experimental investigation of preol isomers, *Fuel* 254 (2019) 115630.
- [36] B. Chen, Z. Wang, J.Y. Wang, H. Wang, C. Toghé, P.E.Á. Alonso, M. Almalki, M. Mehl, W.J. Pitz, S.W. Wagnon, G. Zhang, G. Kukkadapu, P. Dagaut, S. Mani Sarathy, Exploring gasoline oxidation chemistry in jet stirred reactors, *Fuel* 236 (2019) 1282–1292.
- [37] W.W. Ayass, E.F. Nasir, A. Farooq, S.M. Sarathy, Mixing-structure relationship in jet-stirred reactors, *Chem. Eng. Res. Des.* 111 (2016) 461–464.
- [38] J. Bugler, A. Rodriguez, O. Herbinet, F. Battin-Leclerc, C. Toghé, G. Dayma, P. Dagaut, H.J. Curran, An experimental and modelling study of n-pentane oxidation in two jet-stirred reactors: the importance of pressure-dependent kinetics and new reaction pathways, *Proc. Combust. Inst.* 36 (2017) 441–448.
- [39] I.O. Antonov, J. Kwok, J. Zádor, L. Sheps, A combined experimental and theoretical study of the reaction OH + 2-butene in the 400–800K temperature range, *J. Phys. Chem. A* 119 (2015) 7742–7752.
- [40] E.R. Ritter, J.W. Bozzelli, THERM: thermodynamic property estimation for gas phase radicals and molecules, *Int. J. Chem. Kinet.* 23 (1991) 767–778.
- [41] S.M. Burke, J.M. Simmie, H.J. Curran, Critical evaluation of thermochemical properties of C1–C4 species: updated group-contributions to estimate thermochemical properties, *J. Phys. Chem. Ref. Data* 44 (2015) 013101.
- [42] Y. Li, H.J. Curran, Extensive theoretical study of the thermochemical properties of unsaturated hydrocarbons and allylic and super-allylic radicals: the development and optimization of group additivity values, *J. Phys. Chem. A* 122 (2018) 4736–4749.
- [43] F. Battin-Leclerc, A. Rodriguez, B. Husson, O. Herbinet, P.A. Glaude, Z. Wang, Z. Cheng, F. Qi, Products from the oxidation of linear isomers of hexene, *J. Phys. Chem. A* 118 (2014) 673–683.
- [44] C.-W. Zhou, Y. Li, E. O'Connor, K.P. Somers, S. Thion, C. Keese, O. Mathieu, E.L. Petersen, T.A. DeVerter, M.A. Oehlschlaeger, G. Kukkadapu, C.-J. Sung, M. Alrfaf, F. Khaled, A. Farooq, P. Dirrenberger, P.-A. Glaude, F. Battin-Leclerc, J. Santner, Y. Ju, T. Held, F.M. Haas, F.L. Dryer, H.J. Curran, A Comprehensive

- experimental and modeling study of isobutene oxidation, *Combust. Flame* 167 (2016) 353–379.
- [45] J. Zádor, J.A. Miller, Unimolecular dissociation of hydroxypropyl and propoxy radicals, *Proc. Combust. Inst.* 34 (2013) 519–526.
- [46] J.C. Loison, J. Daranlot, A. Bergeat, F. Caralp, R. Mereau, K.M. Hickson, Gas-phase kinetics of hydroxyl radical reactions with C_3H_6 and C_4H_8 : product branching ratios and OH addition site-specificity, *J. Phys. Chem. A* 114 (2010) 13326–13336.
- [47] E.J. Feltham, M.J. Almond, G. Marston, K.S. Wiltshire, N. Goldberg, Reactions of hydroxyl radicals with alkenes in low-temperature matrices, *Spectrochim. Acta Part A Mol. Biomol. Spectrosc.* 56 (2000) 2589–2603.
- [48] H.J. Curran, Rate constant estimation for C1 to C4 alkyl and alkoxy radical decomposition, *Int. J. Chem. Kinet.* 38 (2006) 250–275.
- [49] F. Buda, R. Bounaceur, V. Warth, P.A. Glaude, R. Fournet, F. Battin-Leclerc, Progress toward a unified detailed kinetic model for the autoignition of alkanes from C4 to C10 between 600 and 1200K, *Combust. Flame* 142 (2005) 170–186.
- [50] L. Cai, H. Pitsch, S.Y. Mohamed, V. Raman, J. Bugler, H. Curran, S.M. Sarathy, Optimized reaction mechanism rate rules for ignition of normal alkanes, *Combust. Flame* 173 (2016) 468–482.
- [51] K. Zhang, C. Banyon, U. Burke, G. Kukkadapu, S.W. Wagnon, M. Mehl, H.J. Curran, C.K. Westbrook, W.J. Pitz, An experimental and kinetic modeling study of the oxidation of hexane isomers: developing consistent reaction rate rules for alkanes, *Combust. Flame* 206 (2019) 123–137.
- [52] S. Sharma, S. Ramans, W.H. Green, Intramolecular hydrogen migration in alkylperoxy and hydroperoxyalkylperoxy radicals: accurate treatment of hindered rotors, *J. Phys. Chem. A* 114 (2010) 5689–5701.
- [53] S.M. Villano, L.K. Huynh, H.H. Carstensen, A.M. Dean, High-pressure rate rules for Alkyl + O_2 reactions. 1. The dissociation, concerted elimination, and isomerization channels of the alkyl peroxy radical, *J. Phys. Chem. A* 115 (2011) 13425–13442.
- [54] S.M. Villano, L.K. Huynh, H.H. Carstensen, A.M. Dean, High-pressure rate rules for alkyl + O_2 reactions. 2. the isomerization, cyclic ether formation, and β -scission reactions of hydroperoxy alkyl radicals, *J. Phys. Chem. A* 116 (2012) 5068–5089.
- [55] C.W. Zhou, J.M. Simmie, K.P. Somers, C.F. Goldsmith, H.J. Curran, Chemical kinetics of hydrogen atom abstraction from allylic sites by $3O_2$; implications for combustion modeling and simulation, *J. Phys. Chem. A* 121 (2017) 1890–1899.
- [56] Y. Li, C.W. Zhou, K.P. Somers, K. Zhang, H.J. Curran, The oxidation of 2-butene: a high pressure ignition delay, kinetic modeling study and reactivity comparison with isobutene and 1-butene, *Proc. Combust. Inst.* 36 (2017) 403–411.
- [57] S.M. Burke, U. Burke, R. Mc Donagh, O. Mathieu, I. Osorio, C. Keesee, A. Morones, E.L. Petersen, W. Wang, T.A. DeVerter, M.A. Oehlschlaeger, B. Rhodes, R.K. Hanson, D.F. Davidson, B.W. Weber, C.J. Sung, J. Santner, Y. Ju, F.M. Haas, F.L. Dryer, E.N. Volkov, E.J.K. Nilsson, A.A. Konnov, M. Alrefae, F. Khaled, A. Farooq, P. Dirrenberger, P.A. Glaude, F. Battin-Leclerc, H.J. Curran, An experimental and modeling study of propene oxidation. Part 2: ignition delay time and flame speed measurements, *Combust. Flame* 162 (2015) 296–314.
- [58] C.F. Goldsmith, S.J. Klippenstein, W.H. Green, Theoretical rate coefficients for allyl + HO_2 and allyloxy decomposition, *Proc. Combust. Inst.* 33 (2011) 273–282.
- [59] M. Döntgen, T.T. Pekkanen, S.P. Joshi, R.S. Timonen, A.J. Eskola, Oxidation kinetics and thermodynamics of resonance-stabilized radicals: the pent-1-en-3-yl + O_2 reaction, *J. Phys. Chem. A* 123 (2019) 7897–7910.
- [60] M. Keçeli, S.N. Elliott, Y.P. Li, M.S. Johnson, C. Cavallotti, Y. Georgievskii, W.H. Green, M. Pelucchi, J.M. Wozniak, A.W. Jasper, S.J. Klippenstein, Automated computational thermochemistry for butane oxidation: a prelude to predictive automated combustion kinetics, *Proc. Combust. Inst.* 37 (2019) 363–371.
- [61] A. Miyoshi, Computational studies on the reactions of 3-butenyl and 3-butenylperoxy radicals, *Int. J. Chem. Kinet.* 42 (2010) 273–288.
- [62] W. Tsang, Thermal decomposition of cyclopentane and related compounds, *Int. J. Chem. Kinet.* 10 (1978) 599–617.
- [63] C.F. Goldsmith, L.B. Harding, Y. Georgievskii, J.A. Miller, S.J. Klippenstein, Temperature and pressure-dependent rate coefficients for the reaction of vinyl radical with molecular oxygen, *J. Phys. Chem. A* 119 (2015) 7766–7779.
- [64] X. Chen, C.F. Goldsmith, A theoretical and computational analysis of the methyl-vinyl + O_2 reaction and its effects on propene combustion, *J. Phys. Chem. A* 121 (2017) 9173–9184.
- [65] CHEMKIN-PRO 15101, Reaction Design, San Diego, 2010.